Tools for genetic manipulation of the endemic fungal pathogen, *Emergomyces africanus,* and the application of a fluorescent reporter strain in infection models

Lucian Duvenage[1,2,3]# , Alisha Chetty[1,2,3], Darren D. Thomson[4], Elizabeth R. Ballou[4], Nelesh P. Govender[5,6], Chad A. Rappleye[7]*, J. Claire Hoving[1,2,3]*

1. CMM AFRICA Medical Mycology Research Unit, Institute of Infectious Disease and Molecular Medicine, Faculty of Health Sciences, University of Cape Town, Cape Town, South Africa
2. Wellcome Centre for Infectious Diseases Research in Africa, Institute of Infectious Diseases and Molecular Medicine, University of Cape Town, Cape Town, South Africa
3. Division of Immunology, Department of Pathology, Faculty of Health Sciences, University of Cape Town, Cape Town, South Africa
4. MRC Centre for Medical Mycology, The University of Exeter, Exeter, United Kingdom.
5. Wits Mycology Division, School of Pathology, Faculty of Health Sciences, University of the Witwatersrand, Parktown, Gauteng, South Africa.
6. National Institute for Communicable Diseases, A Division of the National Health Laboratory Service, Johannesburg, Gauteng, South Africa
7. Department of Microbiology, Ohio State University, Columbus, OH, USA

*(CAR and JCH are co-senior authors)

Address correspondence to: Lucian Duvenage, lucian.duvenage@uct.ac.za

Running title: Molecular tools for Emergomyces africanus

Abstract

Emergomyces africanus is a thermally dimorphic fungal pathogen endemic to Southern Africa which can cause fatal systemic infections in persons with advanced HIV disease. Its mechanisms of pathogenesis are not well understood. Characterisation of virulence traits in this pathogen requires appropriate molecular tools for genetic manipulation. Molecular technologies developed for the transformation of *H. capsulatum* were adapted for use in *E. africanus. Agrobacterium*-mediated transformation was used to generate a reporter strain expressing green fluorescent protein (GFP). The *E. africanus* GFP reporter strain facilitated the study of yeast interaction with macrophages *in vitro* and allowed the identification of infected phagocyte cell types in the mouse lung by flow cytometry. *E. africanus* could also maintain episomal plasmids with telomere-like sequences, to introduce expression constructs without genome modification. Using this plasmid system, RNA interference constructs were used to knock down the expression of cell wall α(1,3)-glucan by targeting the transcripts of the α-glucan synthase (*AGS1*). An episomal CRISPR/Cas9 system was evaluated for *E. africanus*, which effectively disrupted *GFP* in a reporter strain and enabled the generation of a *URA5* uracil auxotroph. These tools and strains will facilitate future studies to elucidate the mechanisms of pathogenesis of *E. africanus.*

Importance

Emergomyces africanus is an opportunistic fungal pathogen affecting persons with advanced HIV disease in South Africa. The biology and pathogenesis of *E. africanus* are not well understood, as the importance of the disease caused by this fungus

(emergomycosis) has only been recognised in recent years and molecular studies have been impaired by the lack of genetic technologies. In this work, we describe tools and methods for the genetic modification of this pathogen, which will accelerate future studies investigating how the fungus causes disease in the human host. These essential tools include (1) the ability to create fluorescent reporter strains, such as the green fluorescent protein *E. africanus* strain described here, which facilitates tracking the spread of the fungus during infection and enhances microscopy studies, (2) methods for knocking down gene expression in *E. africanus*, and (3) the permanent disruption of genes through CRISPR/Cas9 gene editing.

Introduction

Emergomyces africanus, part of the recently classified genus *Emergomyces* (1), is a fungal pathogen of humans endemic to Southern Africa (2). The fungus can cause life-threatening systemic infection in immunocompromised individuals, which, in South Africa, has exclusively been persons with advanced HIV disease (3). Because this pathogen is less often suspected by clinicians, patients affected by emergomycosis often are diagnosed only at the late stages of infection, characterised by widespread skin lesions. An understanding of its biology and host-pathogen interaction is needed to develop effective diagnostics and treatment strategies for this infection in high-risk populations.

E. africanus is a thermally dimorphic fungus. It exists in a saprobic mycelial phase in soil and releases airborne conidia (4), which, when inhaled by the host, transition to a yeast phase triggered by body temperature (5). The mechanisms by which these yeast infect host cells are unknown. The ability to genetically manipulate a fungal pathogen

85 can open new avenues of research, whether by examining the effects of gene
86 deletions or introducing reporter genes for a wide range of applications, such as
87 facilitating the detection of the pathogen in infection models. New tools or protocols
88 must be developed or adapted for non-model fungi such as *E. africanus.* In this study,
89 we used molecular tools originally developed for *Histoplasma capsulatum* and other
90 dimorphic fungi (6-11) and adapted them to the genetic modification of *E. africanus*.

91 In some fungi, notably the dimorphic fungal pathogens, homologous recombination is
92 inefficient which prevents gene replacement strategies. In these cases,
93 *Agrobacterium*-mediated gene transfer (ATMT) has been employed to introduce genes
94 of interest (9, 11) or fluorescent transcriptional reporters or to create random insertion
95 libraries for phenotypic screening. Co-culture of *A. tumefaciens,* harbouring the shuttle
96 plasmid, with the fungus results in the insertion of a single copy (in the majority of
97 cases) of the T-DNA randomly in the genome (12). This method has been used
98 successfully for several of the thermally dimorphic pathogens, including *Histoplasma*
99 *capsulatum, Blastomyces dermatitidis, Paracoccidioides brasiliensis* and *Talaromyces*
100 *marneffei* (as reviewed in (13)). We used ATMT to introduce a GFP transgene into *E.*
101 *africanus,* using shuttle vectors and a protocol previously developed for the
102 transformation of *H. capsulatum* (14). The *E. africanus* GFP reporter strain facilitated
103 imaging of yeast-macrophage interactions and identification of phagocyte cell types in
104 the lung associated with the yeast in the mouse model of infection (15) by flow
105 cytometry analysis.

106 Shuttle vectors which replicate in *E. coli* can be maintained by *H. capsulatum* as linear
107 plasmids through the addition of telomere sequences (16-18). These vectors are
108 useful for introducing expression constructs without genome modification. For
109 example, RNA interference (RNAi) constructs can be used to knock down expression

110 of virulence-associated genes (7, 18-22). These plasmids are rapidly lost without
111 selection pressure, which is useful when transient expression is desired, e.g.
112 expression of the genome-modifying enzyme Cas9. Gene deletion/mutation is a
113 powerful tool to study putative virulence-associated traits. CRISPR-Cas9 genome
114 editing has been applied to study these traits in thermally pathogenic fungi, including
115 *Blastomyces dermatitidis (23)* and *Histoplasma capsulatum (6, 24).* In this study, we
116 applied an episomal plasmid system designed for *H. capsulatum* for CRISPR-Cas9
117 genome editing (6) in *E. africanus* to delete distinct genes in the genome.

118 With effective molecular genetic tools in place, and their application optimised for *E.*
119 *africanus*, its virulence traits and pathogenesis can be investigated in future work. This
120 knowledge could facilitate the development of more specific diagnostic tests for early
121 screening of at-risk patients or inform clinical management of the disease.

122

123 **Results and Discussion**

124 **Generation of fluorescent strains using *Agrobacterium*-mediated**
125 **transformation of a GFP transgene**

126 We used *Agrobacterium tumefaciens*-mediated transformation (ATMT) to transform *E.*
127 *africanus* using the shuttle vector pAG22, which encodes a GFP transgene. GFP and
128 hygromycin phosphotransferase are expressed under the control of *H. capsulatum*
129 regulatory elements: *TEF1* (translation elongation factor) constitutive promoter and
130 *TUB2 (tubulin)* terminator, and *RPL1B* (large ribosomal subunit protein) promoter and
131 *RPL7* (large ribosomal subunit protein) terminator, respectively (Figure S1).
132 Transformation of *E. africanus* using *A. tumefaciens* LBA1100 or EHA105 strains
133 carrying pAG22 yielded similar numbers of transformants. Following transformation,

134 individual transformants were screened for GFP expression levels, as insertion of the
135 T-DNA in different loci can result in varying levels of GFP expression (12). To identify
136 reporter strains with high GFP expression, transformant colonies were grown in liquid
137 BHI broth and inspected by fluorescence microscopy. Figure 1 shows an example of
138 differences in GFP fluorescence levels between two transformants.

139 One pAG22 transformant with high fluorescence was selected for further applications.
140 In preliminary experiments with the mouse model of infection, it was noted that the
141 virulence of laboratory-passaged *E. africanus* (including untransformed wild-type
142 strains) was reduced, as higher doses of yeast were required to replicate pathology
143 compared to previous work. Therefore, all wild-type and control strains used in this
144 study were passaged under the same conditions in the laboratory as would be required
145 to generate respective transformants. An intranasal dose of 1×10^7 yeast cells was
146 then used to infect mice, as this could replicate the pathology seen in previous work
147 (15). The GFP fluorescent strain retained pathogenesis compared to the passage-
148 matched wild-type strain in survival studies (Figure S2).

149

150 **Fluorescent E. africanus yeast interaction with macrophages**

151 The GFP-fluorescent yeast facilitated imaging of *E. africanus* interaction with
152 macrophages. J774A.1 macrophages in chambered imaging slides were infected with
153 *E. africanus* yeast (MOI=1) and imaged every 20 minutes. Un-opsonised yeast cells
154 are readily phagocytosed, and a high proportion of yeast cells were intracellular at the
155 start of imaging, one hour following yeast addition. We hypothesise that *E. africanus*
156 may be taken up by macrophages by the same mechanism as *H. capsulatum*, namely,
157 recognition of heat shock protein 60 (Hsp60) on the surface of yeast cells by

158 complement receptor 3 (CD11b/CD18) of macrophages (25), as Hsp60 is highly
159 conserved between the two species. Intracellular yeast could easily be observed by
160 their GFP fluorescence (Figure 2A). Budding of intracellular yeast could be measured
161 in the time-lapse data demonstrating phagocytosed E. africanus yeasts remained
162 viable. The observed budding time of intracellular yeast was not significantly different
163 to that of extracellular yeast in the same proximity (Figure 2B). Yeast cells continued
164 to proliferate intracellularly over time, with some macrophages appearing heavily
165 infected and unable to control yeast proliferation. These data indicate that the
166 intracellular niche is permissive to *E. africanus* replication, as it is for *H. capsulatum.*
167 Previous work showed that bone marrow-derived macrophages are not actively lysed
168 by *E. africanus*, unlike *H. capsulatum*, which may be due to the non-lytic activity of the
169 *E. africanus* Cbp1 homologue (26). These data suggest that, similar to *H. capsulatum*
170 and *P. brasiliensis,* non-activated phagocytes are unable to control *E. africanus,* which
171 may aid in fungal systemic dissemination during infection (27, 28). Further studies
172 using the GFP reporter strain and live cell imaging could provide more information on
173 the dynamics of intracellular replication and macrophage cell death.

174

175 **Identification of infected phagocyte populations in the mouse lung following**
176 **infection with the GFP reporter strain**

177 We applied the GFP fluorescent *E. africanus* strain to examine its association with
178 phagocytes *in vivo.* Mice were infected intranasally with the fluorescent *E. africanus*
179 strain, and after 7 days, myeloid cell recruitment in the lungs was analysed by flow
180 cytometry. Lungs from uninfected mice were analysed as a control. Gating first on
181 GFP+ cells (i.e., cells with internalised E. africanus) showed that <1% of GFP+ cells

182 were CD45-negative (Figure 3A), suggesting that nearly all phagocytosed *E. africanus*
183 yeasts resided in CD45+ phagocytes. Similar results were reported in a study with an
184 *H. capsulatum* GFP-expressing strain (29), suggesting that both pathogens persist
185 well within this intracellular niche *in vivo*. However, these results only reflect the
186 intracellular fungal burden at the day 7 timepoint, and do not account for fungi that
187 may have been cleared by this time. Most GFP-fluorescent yeasts were associated
188 with neutrophils (CD11b^{hi}, Ly6G^{hi}) (66.4±17.4% of GFP+ cells; Figure 3B). The
189 remainder of cell types that contained GFP yeast were interstitial macrophages
190 (10.3±5.3%), dendritic cells (MHCII^{hi}, CD11c+) (2.1±0.7%) and a very small subset of
191 CD11b-, CD11c- cells (Figure 3B).

192 Alternatively, gating first on all live host cells showed what proportion of total cells were
193 infected with *E. africanus* (GFP+). Of CD45+ cells within the lung, approximately
194 16.4±4% were infected (GFP+). We then characterised the GFP-fluorescent (i.e.,
195 infected) proportion of each myeloid cell type, using a similar gating strategy. The
196 mean proportion of DCs that were infected (GFP-positive) was 57.3±4.3% of DCs
197 detected (MHCII^{hi}, CD11c^{hi}), with smaller proportions of total lung macrophages and
198 neutrophils infected (Figure 3C). Similar proportions were reported for *H. capsulatum*
199 with the distribution of GFP-fluorescent *H. capsulatum*-infected phagocytes at day 7
200 post-infection: macrophages: 25.1%, PMNs: 51.2% and DCs: 24.3% for the G217B
201 strain (29). DCs are pivotal in the adaptive immune response to fungi, including *H.*
202 *capsulatum* (30, 31). The high proportion of DCs infected with *E. africanus* at the 7-
203 day timepoint suggests the initiation of adaptive immunity. The cellular recruitment (of
204 CD45+ cells) to the lung in response to the GFP-fluorescent strain was not significantly
205 different to CD45+ cell populations in animals infected with the non-fluorescent wild-
206 type control (Figure 3D), indicating the GFP-fluorescent E. africanus strain stimulates

207 a similar host immune response. Previous work examined myeloid cell recruitment in
208 *E. africanus*-infected mouse lung at 14 days post-infection, although a lower dose of
209 yeast was used for infection (15). A time course of infection was not performed in the
210 current study; this could be included in future experiments to gain more information on
211 cell recruitment and infected phagocyte proportions over time.

212 SiglecF+ alveolar macrophages were detected in lungs from uninfected mice (1.5-4%
213 of total cells) but the proportion was reduced in infected mice (0.01-0.16% of total
214 cells). Similarly, the number of interstitial macrophages and dendritic cells was higher
215 in uninfected mice (Figure 3D). This could be due to the proportional increase in
216 neutrophils recruited or apoptosis of leukocytes in the lung, a known feature of
217 infection with *H. capsulatum* and a critical element of protective immunity (32).

218

219 **Transformation of *E. africanus* with episomal vectors and reduction of cell wall**
220 **α(1,3)-glucan by RNA interference**

221 *E. africanus* could be transformed with episomal plasmids based on pCR115 (18) for
222 which linear plasmids with telomeres are maintained without chromosome integration.
223 This was first tested by constructing a modified plasmid with hygromycin B selection
224 (pHygR-GFP). The number of colonies obtained using electroporation of episomal
225 plasmids was typically lower than for ATMT. Hygromycin selection pressure was
226 maintained when working with these transformants, as these plasmids are rapidly lost
227 from the cell population without selection.

228 To silence production of α(1,3)-glucan in *E. africanus*, we expressed an AGS1-
229 targeting RNA hairpin from an episomal plasmid based on the AGS1-RNAi plasmid
230 pCR115. The RNA hairpin is designed for RNAi-induced knockdown of the *H.*

231 *capsulatum AGS1* gene, with homology to a 678 base pair region of exon 3 of this
232 gene (18). This region is 84% similar overall in *H. capsulatum* and *E. africanus,* with
233 several continuous sections of at least 20 nucleotides or with 100% identity. Therefore,
234 we hypothesised that effective RNAi silencing using the same RNA hairpin could be
235 achieved in *E. africanus,* given that several 21-22 small interfering RNA molecules
236 with complete sequence match are produced following Dicer processing of the long
237 double-stranded RNA. We replaced the GFP in pHygR-GFP with the *AGS1* inverted
238 repeat sequence from pCR115 and used this plasmid (pHygR-HcAGS1-RNAi) to
239 transform *E. africanus.* Yeast transformed with pHygR-HcAGS1-RNAi did not differ in
240 growth rate compared to control yeast, which was transformed with a similar plasmid
241 containing a GFP inverted repeat.

242 Reduction of cell wall α(1,3)-glucan through RNA interference was assessed by
243 staining the AGS1-RNAi plasmid-transformed yeasts with a monoclonal antibody
244 recognising α(1,3)-glucan. It was noted that not all yeast cells were uniformly stained
245 (Figure 4A) suggesting variable amounts of α(1,3)-glucan. *H. capsulatum* also displays
246 variation in cell wall α(1,3)-glucan levels, as assessed by staining with the same
247 antibody, during broth culture growth (33). Similarly, *E. africanus* cell wall α(1,3)-glucan
248 levels may increase at different time points during culture, or in different growth media.
249 Nevertheless, yeasts transformed with the *AGS1* RNAi plasmid showed an overall
250 lower level of cell wall α(1,3)-glucan staining in the population compared to the control
251 (Figure 4A and 4B). RNAi-induced gene silencing does not typically lead to a complete
252 knockdown of the target, and due to variability in dsRNA expression, a small proportion
253 of cells do not exhibit the full RNAi effect (18). Therefore, some α(1,3)-glucan staining
254 was still observed in *E. africanus* yeasts maintaining the RNAi plasmid.

255

256 **Gene mutation in *E. africanus* using an episomal CRISPR/Cas9 system**

257 To test whether CRISPR-Cas9 gene editing could facilitate gene mutation in E.
258 africanus, we transformed a GFP-expressing strain of *E. africanus* with a linear
259 plasmid expressing Cas9 and a GFP-targeting CRISPR gRNA. The GFP-fluorescent
260 *E. africanus* strain was generated through ATMT using pAG21 (GFP-expression and
261 G418 selection). The CRISPR-Cas9 plasmid provided for hygromycin resistance and
262 expressed a gRNA targeting the GFP gene. Hygromycin-resistant transformant
263 colonies were passaged in BHI broth with hygromycin B selection, and the yeasts were
264 examined by fluorescence microscopy for loss of the GFP fluorescence. After
265 successive passages, an increasing proportion of the population was no longer GFP
266 fluorescent (Figure 5A). Sequencing of the GFP gene in the transformant population
267 confirmed a mixed population with indels at the expected Cas9 cut site (Figure 5B)
268 showing efficient CRISPR/Cas9-based genome editing in *E. africanus*.

269 Auxotroph strains are useful for genetic manipulations because they facilitate selection
270 of plasmids carrying genes that rescue the auxotrophy. A previous CRISPR/Cas9
271 workflow used for *H. capsulatum* (6) was used to disrupt *URA5* in *E. africanus* to
272 generate a uracil auxotroph strain. The *E. africanus URA5* homologue (Gene:
273 ACJ72_02173) was identified through a BLAST search. The protein sequence is highly
274 similar to that of *H. capsulatum* (88.1% identity, 93.0% similarity as determined by
275 pairwise alignment using EMBOSS Water (34)). A guide RNA sequence was designed
276 using CRISPOR (https://crispor.gi.ucsc.edu/) (35) to maximise the chance of indel
277 generation in the *URA5* gene while minimising off-target effects. Following
278 transformation of wild-type *E. africanus* with the URA5-targeting CRISPR-Cas9
279 plasmid, followed by four passages under hygromycin selection, uracil auxotrophs
280 were selected using 5-FOA-resistance screening. Several 5-FOA-resistant clones

281 were identified, and their inability to grow without uracil was validated by failure to grow
282 in media lacking uracil. Sequencing of four clones showed a single nucleotide T
283 insertion in all clones (Figure 5C), causing a frameshift mutation, preventing
284 production of a functional *URA5* gene product. This *E. africanus ura5*-mutant can now
285 be used as the host for *URA5*-based expression vectors or RNAi vectors. These
286 vectors are also stable *in vivo,* as evidenced by continued virulence*; H. capsulatum*
287 uracil auxotrophs are avirulent in mice, which is likely to be the case for *E. africanus*
288 as well (36).

289

290 **Conclusions**

291 In this study, we demonstrate that molecular tools developed for genetic modification
292 of *H. capsulatum* could be adapted for use in *E. africanus,* suggesting that the two
293 species use similar regulatory elements for high-level gene expression. Our results
294 include the use of ATMT to transform *E. africanus* with expression plasmids,
295 generating a GFP-fluorescent strain that can be used for tracking infections both in
296 cultured macrophages and *in vivo*. In addition, we provide results showing the efficacy
297 of episomal plasmids designed to induce RNA-interference-based gene knock-down
298 and CRISPR-Cas9-based mutation of target genes. Thus, by adapting technologies,
299 we have put into place tools and methodologies to functionally study genes in E.
300 africanus through expression as well as loss-of-function. Furthermore, we have
301 created an *E. africanus* uracil auxotroph strain enabling the use of URA5-based
302 complementation vectors instead of hygromycin selection. Such URA5-based vectors
303 have the advantage of providing for selection *in vivo*, which cannot be done with

304 hygromycin. Together, these tools make *E. africanus* amenable to genetic modification
305 to investigate virulence traits and how they influence the host-pathogen interaction.

306

307 **Materials and Methods**

308 ***E. africanus* and *A. tumefaciens* strains and growth conditions**

309 *Emergomyces africanus* (clinical isolate CBS 136260 (4)) was grown in brain-heart
310 infusion broth (BHI) (Cat No. 110493, Merck, USA), at 37 °C, 180 rpm, or maintained
311 on BHI agar plates (Cat. No. 70138, Merck) at 37 °C. *A. tumefaciens* strains LBA1100
312 and EHA105 was maintained on LB agar plates at 25 °C. Transformation of
313 *Agrobacterium* binary vectors into *A. tumefaciens* was done by electroporation as
314 described in (37) and transformants selected with 100 ug/mL kanamycin.

315

316 **Transformation using *Agrobacterium tumefaciens***

317 Transformation of *E. africanus* yeast by *Agrobacterium* was done using previously
318 established methods for *H. capsulatum* (14), with the exception that BHI broth or BHI
319 agar plates were used instead of *Histoplasma*-specific growth medium. *Agrobacterium*
320 *tumefaciens* strains LBA1100 and EHA105 were used to transform *E. africanus* with
321 pAG22 (GFP-expression, hygromycin resistance), yielding similar results. BHI was
322 inoculated with a colony of *E. africanus* from a fresh streak plate, and the culture was
323 grown for three days at 37 °C with shaking. Colonies from a streak plate of *A.*
324 *tumefaciens* were used to inoculate 5 ml minimal glucose medium (14) for 24 h at
325 25 °C, then 1 ml of this culture was used to inoculate 5 ml induction medium containing
326 0.1 mM acetosyringone (Sigma-Aldrich) for a further 16 h growth. *E. africanus* yeast

327 cells were washed with PBS by centrifugation and resuspension, then resuspended in
328 induction medium. The optical density (600 nm) of both *E. africanus* and *A.*
329 *tumefaciens* suspensions was determined, then combined in 900 µl to give final optical
330 densities of 1.0 for each. Suspensions OD600=1.0 have approximately 5×10^8 cells/ml
331 and 2.5×10^8 cells/ml of *A. tumefaciens* and *E. africanus,* respectively, giving an MOI
332 of 2:1. The co-culture was applied dropwise to sterile Whatman No. 5 qualitative filter
333 papers placed on co-cultivation plates. The co-cultivation plates were incubated at 25
334 °C for 2 days, then transferred to BHI agar plates containing 300 µg/ml hygromycin B
335 and 200 µM cefotaxime. The plates were incubated at 37 °C for 10-14 days until *E.*
336 *africanus* transformant colonies appeared. Single colonies were picked and streaked
337 on fresh BHI plates containing 300 µg/ml hygromycin B. From these plates, single
338 colonies were used to inoculate BHI broth to grow liquid cultures of individual
339 transformants. Glycerol stocks (20%) of liquid cultures were preserved at -80 °C.

340

341 **Infection of macrophages with *E. africanus* and live-cell imaging**

342 J774A.1 murine macrophage cells (ATCC: TIB-7) were seeded at a density of 2×10^5
343 cells in 0.3 ml macrophage medium (DMEM high glucose GlutaMAX®, 10% FBS,
344 penicillin/streptomycin [Gibco]) in 8-well imaging slides (ibidi GMBH, Cat. No. 80826)
345 24 h prior to the addition of *E. africanus* yeast. *E. africanus* yeast was grown for 3 days
346 in BHI broth, then washed with PBS and counted using a haemocytometer. 2×10^5
347 yeast cells in 300 µl macrophage media were added to macrophages in imaging slides
348 to achieve a ratio of one yeast cell per macrophage (MOI=1). The slides were then set
349 up for time-lapse imaging under the conditions of 37 °C, 5% CO_2. Imaging was started
350 1 hour post-yeast addition. Imaging was done using a Zeiss AxioObserver

351 fluorescence microscope at 40X magnification. Analysis of observed budding time was
352 done by examining yeast cells that were intracellular or extracellular, at t=0, with no
353 visible buds.

354

355 **Mouse model of infection and flow cytometry**

356 To examine the responses to *E. africanus* in the mouse lung, three groups of mice
357 were analysed (n=6 per group): (1) uninfected mice, (2) mice infected with the wild-
358 type clinical isolate and (3) mice infected with the GFP fluorescent *E. africanus* strain.
359 Eight- to twelve-week-old male CL57/B6 mice were obtained from the University of
360 Cape Town Animal Research Specific Pathogen Free Facility. *E. africanus* wild-type
361 and GFP fluorescent strains were grown in BHI broth for 3 days at 37 °C until OD600
362 reached approximately 1.0. Yeast cells were washed twice with PBS before counting
363 using a haemocytometer. Mice were anaesthetised with ketamine and xylazine (80
364 mg/kg and 16 mg/kg, respectively), then infected intranasally with 50 µl of yeast cell
365 suspension containing 1×10^7 yeast cells. Animal welfare was monitored daily. After 7
366 days, mice were euthanised by halothane inhalation and the lungs were removed and
367 stored in DMEM + 5% FBS on ice. Lungs were digested in digestion buffer (15)
368 containing 50 units/ml Collagenase Type I and 13 µg/ml DNAseI for 1h at 37 °C. The
369 digested lungs were passed through a 70 µm cell strainer using a sterile syringe
370 plunger. This process was repeated using a 40 µm cell strainer. Red blood cells were
371 lysed using 1x RBC lysis buffer (eBioscience), then remaining cells collected by
372 centrifugation and resuspension in DMEM + 5% FBS, then counted using
373 haemocytometer. 2×10^6 cells per well were added to a V-bottom 96-well plate.
374 Myeloid cells were stained in MACS buffer (0.5% BSA, 2 mM EDTA in PBS) using the

375 antibodies in Table 3, together with 1% Fc block and 2% heat-inactivated rat serum,
376 for 20 min at 4 °C in the dark, then washed twice with MACS buffer. 7-AAD (Biolegend)
377 was used as the cell viability stain. Single-stained and unstained controls were used
378 to compensate for spectral overlap. Stained cells were analysed by flow cytometry
379 using an LSR Fortessa™ (BD Immunocytometry Systems, San Jose, CA, USA) and
380 BD FACS Diva software (v6.0). Flowjo software (v10.0.7) (Treestar, Ashland, OR,
381 USA) was used for post-acquisition analysis cell population determination. The gating
382 strategy used is shown in Figure 3A.

383

384 **Ethics statement**

385 All work with mice was done with ethical clearance from the University of Cape Town
386 Animal Research Ethics Committee, reference numbers 020/017 and 024/014.

387

388 **Statistical analysis and software**

389 Values are reported as means ± standard deviation. Differences between groups were
390 determined using a two-tailed Student's t-test or one-way ANOVA using GraphPad
391 Prism v10.6.1. Plasmid map generation and alignments of DNA sequence data were
392 done using SnapGene v8.02. ImageJ 1.54p was used for image analysis (mean
393 fluorescence intensities and total cell counting).

394

395 **Plasmid construction**

396 Plasmids pAG21, pAG22, pCR115 (18), pSL01 and pCR745 (6) were provided by
397 CAR. Isolation of plasmid DNA, restriction enzyme cloning and PCR/gel purification

398 was done using standard methods, and plasmids were maintained in *E. coli* DH5α.
399 Restriction enzymes and ligation kits were purchased from New England Biolabs. An
400 episomal GFP expression plasmid (pHygR-GFP) was constructed by digestion of
401 pAG22 with EcoRI and HindIII, and ligating the fragment containing the GFP- and *hph*
402 expression cassettes into the similarly-digested pCR115 vector backbone. To
403 construct pHyg-HcAGS1-RNAi (AGS1 inverted repeat) used for *AGS1* RNAi, the *GFP*
404 sequence from plasmid pHygR-GFP was exchanged with the *AGS1* inverted repeat
405 sequence from pCR115 by digestion with AscI and SpeI. A control *GFP* RNAi plasmid
406 (pHygR-GFP-RNAi) was constructed by inserting an inverted repeat of *GFP* into
407 pHygR-GFP by PCR with GFP-SpeI-F and XhoI-GFP-R primers and restriction
408 enzyme cloning. For CRISPR/Cas9-mediated disruption of GFP, plasmid pCR115-
409 sgGFP was created: a portion of plasmid pCR745 (6) containing the guide RNA
410 targeting GFP, was digested with SwaI and AvrII and ligated into similarly digested
411 pSL01 (6), resulting in plasmid pSL01-sgGFP. For CRISPR/Cas9-medited disruption
412 of *URA5,* a synthetic DNA sequence containing the guide RNA sequence,
413 hammerhead and HDV ribozyme sequences, and part of the tracr RNA sequence,
414 including 15 bp up- and downstream-homology regions was designed for cloning into
415 pSL01 as described in (6). The guide RNA sequence was designed using CRISPOR
416 (https://crispor.gi.ucsc.edu/) (35) to maximise the chance of indels while preventing
417 off-target effects. This sequence was synthesised by Integrated DNA Technologies
418 (Leuven, Belgium). The synthetic DNA sequence was cloned into SwaI-digested
419 pSL01 and transformed into competent *E. coli* cells using In-Fusion® HD Cloning Kit
420 (Takara Bio) using the manufacturer's recommendations. Table 1 summarises the
421 plasmids used in this study.

422

423 **Transformation of yeast with episomal plasmids by electroporation**

424 Transformation of *E. africanus* with plasmids by electroporation of was based on
425 previously established methods for *H. capsulatum* (17). Briefly, *E. africanus* yeasts
426 were grown in 5 ml BHI broth for 3 days until OD600 reached approximately 1.0. Yeast
427 cells were collected by centrifugation and resuspended in 2 ml 10% mannitol.
428 Plasmids were linearised by digestion with PmeI to expose the telomeres, then
429 column-purified and eluted with nuclease-free water. Three hundred microlitres of *E.*
430 *africanus* yeast suspension (1×10^7 yeast cells) was mixed with 200 ng purified
431 plasmid in a chilled electroporation cuvette (0.2 cm gap), then electroporated in a
432 single pulse using a Bio-Rad Gene Pulser® II system with the following settings: 1.25
433 kV, 50 mF, 600 Ω, which gave a time constant of 8-12 ms. Following electroporation,
434 500 µl of BHI broth was mixed with cells and this cell suspension was applied dropwise
435 to sterile Whatman No. 5 qualitative filter papers placed on BHI agar plates with no
436 selection. These plates were incubated for 48 h at 37 °C to allow for recovery of
437 transformants, before transferring the membranes to BHI agar plates containing 300
438 µg/ml hygromycin B. The plates were incubated at 37 °C for 10-14 days until
439 transformant colonies appeared. Single colonies were picked and streaked onto fresh
440 BHI plates (300 µg/ml hygromycin B). Selection with hygromycin B (300 µg/ml) was
441 maintained for growing liquid cultures, after which -80 °C glycerol stocks were
442 prepared for long-term storage of strains, as described above.

443

444 **Cell wall alpha(1,3)-glucan staining of RNAi strains**

445 Yeasts harbouring the *AGS1* RNAi plasmid pHygR-HcAGS1-RNAi or the control
446 plasmid pHygR-GFP-RNAi were grown for 3 days in BHI broth with 300 µg/ml

447 hygromycin B until cell density reached an OD600 of 1.0. Cells from 300 µl of culture
448 were collected by centrifugation, then washed twice with PBS, and fixed in 4%
449 paraformaldehyde overnight at 4 °C. Cells were washed twice with PBS, then blocked
450 with 1% BSA, PBS for 1 h. Cells were then stained with 1:150 mouse IgM MOPC-
451 104E antibody (M5170, Sigma-Aldrich) in 1% BSA, PBS for 2 h at ambient
452 temperature. The cells were washed twice by centrifugation and resuspended in PBS
453 and stained with 1:400 anti-mouse IgM secondary antibody conjugated to
454 AlexaFluor488 (Invitrogen, A-21042) for 1 h at ambient temperature. To stain total
455 yeast cells, calcofluor white was added at a final concentration of 100 µg/ml and
456 incubated for 15 min at ambient temperature in the dark. Cells were washed twice with
457 PBS and resuspended in 20 µl PBS. A 5µl sample of stained cells was spotted onto a
458 microscope slide, allowed to air-dry and mounted with ProLong™ Glass Antifade
459 Mountant (P36984, Invitrogen). The slides were examined using a Zeiss Axiovert
460 200M fluorescence microscope with a monochrome Zeiss AxioCam HRm camera at
461 100x magnification. Exposure times were kept constant for all samples when capturing
462 images for mean fluorescence analysis. Fluorescence of the population was
463 determined by measuring the background-corrected mean grey values for 10 fields of
464 view each using ImageJ, for two pooled independent experiments, then dividing this
465 value by the number of total cells (as determined by calcofluor white staining).

466

467 **Targeted mutagenesis using CRISPR/Cas9-plasmids**

468 A GFP-expressing strain of *E. africanus* was generated through ATMT using pAG21
469 (equivalent to pAG22 but with a G418 resistance marker instead of hygromycin B
470 resistance). The GFP-fluorescent strain was subsequently transformed with PmeI-

471 linearised plasmid pSL01-sgGFP by electroporation. Hygromycin-resistant
472 transformant colonies were picked and grown in BHI broth for successive passages
473 (1:50 dilution), maintaining hygromycin selection every 3 days. Samples of these
474 cultures were examined by fluorescence microscopy for GFP expression. For DNA
475 sequencing, yeast cells from 1 ml of culture was collected by centrifugation, lysed with
476 200 µl of lysis buffer (2% Triton X-100, 20 mM EDTA) and beating (2 min) with
477 approximately 100 µl of glass beads (0.5 µm diameter). 100 µL of phenol and 100 µl
478 chloroform-isoamyl alcohol (25:24:1) were added, and the phases were separated by
479 centrifugation. DNA was recovered by transferring 50 µl of the aqueous (upper) phase
480 into 200 µl distilled water. This crude DNA-containing solution was used as the
481 template (2% vol/vol) for PCR using Taq polymerase and primers flanking the
482 expected gene editing sites: GFP-SpeI-F and GFP-Xho-R, or Ura seq-F and Ura seq-
483 R.

484 For mutation of *URA5* to create a uracil auxotroph, a guide RNA sequence targeting
485 URA5 was designed using CRISPOR (https://crispor.gi.ucsc.edu/) (35). A DNA
486 construct containing the crRNA, hammerhead- and HDV ribozyme sequences, and
487 part of the tracrRNA sequence, with 15 bp flanking homology arms, was synthesised
488 as described in (6) for cloning into plasmid pSL01, by Integrated DNA Technologies
489 (Leuven, Belgium). The sequence of this construct is shown in Table 2. Cloning of this
490 synthetic DNA into SwaI-digested plasmid pSL01 was done through InFusion Cloning
491 (Takara Biotec) as per the manufacturer's recommendations. Constructs were verified
492 through Sanger sequencing. *E. africanus* was transformed with this plasmid by
493 electroporation as described above, followed by selection with hygromycin B. After
494 four passages in liquid culture, cultures were streaked onto BHI plates supplemented
495 with 1mg/ml 5-Fluoroorotic Acid (5-FOA, R0811, ThermoFisher) and 100 µg/ml uracil

496 to isolate uracil auxotrophs. Uracil auxotrophy was confirmed by the inability to grow
497 in DMEM/F12 media (11320033, Gibco), which lacks uracil, compared to growth in
498 parallel in DMEM/F12 media supplemented with 100 µg/ml uracil. Independent clones
499 were picked for Sanger sequencing.

500

501

502 Table 1: Plasmids used in the study

503

Plasmid	Application	Selection
pAG22	ATMT	Hygromycin B (300 µg/ml)
pAG21	ATMT	G418 (1 mg/ml)
pCR115	*AGS1* RNAi	[Uracil auxotrophy]
pHygR-GFP	GFP episomal plasmid	Hygromycin B (300 µg/ml)
pHygR-GFP-RNAi	GFP inverted repeat plasmid (RNAi control)	Hygromycin B (300 µg/ml)
pHygR-HcAGS1-RNAi	*AGS1* RNAi	Hygromycin B (300 µg/ml)
pCR745	CRISPR/Cas9	[Uracil auxotrophy]
pSL01	CRISPR/Cas9	Hygromycin B (300 µg/ml)
pSL01-sgGFP	CRISPR/Cas9	Hygromycin B (300 µg/ml)
pSL01-sgURA	CRISPR/Cas9	Hygromycin B (300 µg/ml)

504

505

506 Table 2: Primers and oligonucleotides

GFP-SpeIF	GAGAACTAGTATGAGCAAGGGCGAGGAGC
GFP-XhoIR	GAGACTCGAGCTTGTACAGCTCGTCCATGC
Synthesised sequence for *URA5* CRISPR/Cas9 mutation (guide sequence underlined)	CTCTCCCAATTTTCACATTTAAATCCCGCC ACCCGATGTCTGATGAGTCCGTGAGGAC GAAACGAGTAAGCTCGTC<u>ACATCGGGTT TCGGAATGG</u>AGTTTTAGAGCTAGAAATAG CAAGTTAAAATAAGGCTAGTCCGTTAT
Ura seq F	TTGACACAGCCCATAAACG
Ura seq R	ATCGCCTTCTATATTCCTCC

507

508

509 Table 3: Flow cytometry antibodies

Target (Clone)	Conjugated fluorophore	Manufacturer (catalogue number)	Dilution
CD45 (30-F11)	BV510	BD Biosciences (567800)	1:100
CD11b (M1/70)	BV421	BD Biosciences (566313)	1:100
CD11c (HL3)	Alexa Fluor 700	BD Biosciences (560583)	1:100
Ly-6G (1A8)	APC	BD Biosciences (560599)	1:100
F4/80 (BM8)	PE/Cy7	Biolegend (123113)	1:100
Siglec-F (E50-2440)	APC/Cy7	BD Biosciences (565527)	1:50
I-A/I-E (MHCII) (M5/114.15.2)	PE/Cy5	Biolegend (107611)	1:100

510

511

512

513

514

515

516

517

518

519

520

521

522

523

524

525

526

527

528

References

1. Dukik K, Munoz JF, Jiang Y, Feng P, Sigler L, Stielow JB, Freeke J, Jamalian A, Gerrits van den Ende B, McEwen JG, Clay OK, Schwartz IS, Govender NP, Maphanga TG, Cuomo CA, Moreno LF, Kenyon C, Borman AM, de Hoog S. 2017. Novel taxa of thermally dimorphic systemic pathogens in the Ajellomycetaceae (Onygenales). Mycoses 60:296-309.
2. Schwartz IS, Govender NP, Sigler L, Jiang Y, Maphanga TG, Toplis B, Botha A, Dukik K, Hoving JC, Munoz JF, de Hoog S, Cuomo CA, Colebunders R, Kenyon C. 2019. Emergomyces: The global rise of new dimorphic fungal pathogens. PLoS Pathog 15:e1007977.
3. Schwartz IS, Kenyon C, Lehloenya R, Claasens S, Spengane Z, Prozesky H, Burton R, Parker A, Wasserman S, Meintjes G, Mendelson M, Taljaard J, Schneider JW, Beylis N, Maloba B, Govender NP, Colebunders R, Dlamini S. 2017. AIDS-Related Endemic Mycoses in Western Cape, South Africa, and Clinical Mimics: A Cross-Sectional Study of Adults With Advanced HIV and Recent-Onset, Widespread Skin Lesions. Open Forum Infect Dis 4:ofx186.
4. Schwartz IS, McLoud JD, Berman D, Botha A, Lerm B, Colebunders R, Levetin E, Kenyon C. 2018. Molecular detection of airborne Emergomyces africanus, a thermally dimorphic fungal pathogen, in Cape Town, South Africa. PLoS Negl Trop Dis 12:e0006174.
5. Jiang Y, Dukik K, Muñoz JF, Sigler L, Schwartz IS, Govender NP, Kenyon C, Feng P, van den Ende BG, Stielow JB, Stchigel AM, Lu H, de Hoog S. 2018. Phylogeny, ecology and taxonomy of systemic pathogens and their relatives in Ajellomycetaceae (Onygenales): Blastomyces, Emergomyces, Emmonsia, Emmonsiellopsis. Fungal Diversity 90:245-291.
6. Rappleye CA. 2023. Targeted gene deletions in the dimorphic fungal pathogen Histoplasma using an optimized episomal CRISPR/Cas9 system. mSphere 8:e0017823.
7. Brechting PJ, Shah C, Rakotondraibe L, Shen Q, Rappleye CA. 2023. Histoplasma capsulatum requires peroxisomes for multiple virulence functions including siderophore biosynthesis. mBio 14:e0328422.
8. Kujoth GC, Sullivan TD, Klein BS. 2020. Gene Editing in Dimorphic Fungi Using CRISPR/Cas9. Curr Protoc Microbiol 59:e132.
9. Kemski MM, Stevens B, Rappleye CA. 2013. Spectrum of T-DNA integrations for insertional mutagenesis of Histoplasma capsulatum. Fungal Biol 117:41-51.
10. Youseff BH, Rappleye CA. 2012. RNAi-based gene silencing using a GFP sentinel system in Histoplasma capsulatum. Methods Mol Biol 845:151-64.
11. Sullivan TD, Rooney PJ, Klein BS. 2002. Agrobacterium tumefaciens integrates transfer DNA into single chromosomal sites of dimorphic fungi and yields homokaryotic progeny from multinucleate yeast. Eukaryot Cell 1:895-905.
12. Idnurm A, Bailey AM, Cairns TC, Elliott CE, Foster GD, Ianiri G, Jeon J. 2017. A silver bullet in a golden age of functional genomics: the impact of Agrobacterium-mediated transformation of fungi. Fungal Biol Biotechnol 4:6.

575 13. Sil A, Andrianopoulos A. 2014. Thermally Dimorphic Human Fungal
576 Pathogens--Polyphyletic Pathogens with a Convergent Pathogenicity Trait.
577 Cold Spring Harb Perspect Med 5:a019794.
578 14. Zemska O, Rappleye CA. 2012. Agrobacterium-Mediated Insertional
579 Mutagenesis in Histoplasma capsulatum, p 51-66, Host-Fungus Interactions
580 doi:10.1007/978-1-61779-539-8_4. Humana Press.
581 15. Hoft MA, Duvenage L, Salie S, Keeton R, Botha A, Schwartz IS, Govender
582 NP, Brown GD, Hoving JC. 2024. The pathogenesis of experimental
583 Emergomycosis in mice. PLoS Negl Trop Dis 18:e0011850.
584 16. Woods JP, Goldman WE. 1993. Autonomous replication of foreign DNA in
585 Histoplasma capsulatum: role of native telomeric sequences. J Bacteriol
586 175:636-41.
587 17. Woods JP, Heinecke EL, Goldman WE. 1998. Electrotransformation and
588 expression of bacterial genes encoding hygromycin phosphotransferase and
589 beta-galactosidase in the pathogenic fungus Histoplasma capsulatum. Infect
590 Immun 66:1697-707.
591 18. Rappleye CA, Engle JT, Goldman WE. 2004. RNA interference in Histoplasma
592 capsulatum demonstrates a role for alpha-(1,3)-glucan in virulence. Mol
593 Microbiol 53:153-65.
594 19. Ray SC, Rappleye CA. 2022. Mac1-Dependent Copper Sensing Promotes
595 Histoplasma Adaptation to the Phagosome during Adaptive Immunity. mBio
596 13:e0377321.
597 20. Shen Q, Ray SC, Evans HM, Deepe GS, Jr., Rappleye CA. 2020. Metabolism
598 of Gluconeogenic Substrates by an Intracellular Fungal Pathogen
599 Circumvents Nutritional Limitations within Macrophages. mBio 11.
600 21. Dade J, DuBois JC, Pasula R, Donnell AM, Caruso JA, Smulian AG, Deepe
601 GS, Jr. 2016. HcZrt2, a zinc responsive gene, is indispensable for the survival
602 of Histoplasma capsulatum in vivo. Med Mycol 54:865-75.
603 22. Hilty J, George Smulian A, Newman SL. 2011. Histoplasma capsulatum
604 utilizes siderophores for intracellular iron acquisition in macrophages. Med
605 Mycol 49:633-42.
606 23. Kujoth GC, Sullivan TD, Merkhofer R, Lee TJ, Wang H, Brandhorst T,
607 Wuthrich M, Klein BS. 2018. CRISPR/Cas9-Mediated Gene Disruption
608 Reveals the Importance of Zinc Metabolism for Fitness of the Dimorphic
609 Fungal Pathogen Blastomyces dermatitidis. mBio 9.
610 24. Joehnk B, Ali N, Voorhies M, Walcott K, Sil A. 2023. Recyclable
611 CRISPR/Cas9-mediated gene disruption and deletions in Histoplasma.
612 mSphere 8:e0037023.
613 25. Long KH, Gomez FJ, Morris RE, Newman SL. 2003. Identification of heat
614 shock protein 60 as the ligand on Histoplasma capsulatum that mediates
615 binding to CD18 receptors on human macrophages. J Immunol 170:487-94.
616 26. Azimova D, Herrera N, Duvenage L, Voorhies M, Rodriguez RA, English BC,
617 Hoving JC, Rosenberg O, Sil A. 2022. Cbp1, a fungal virulence factor under
618 positive selection, forms an effector complex that drives macrophage lysis.
619 PLoS Pathog 18:e1010417.
620 27. Allendoerfer R, Deepe GS, Jr. 1997. Intrapulmonary response to Histoplasma
621 capsulatum in gamma interferon knockout mice. Infect Immun 65:2564-9.
622 28. Calich VL, da Costa TA, Felonato M, Arruda C, Bernardino S, Loures FV,
623 Ribeiro LR, de Cássia Valente-Ferreira R, Pina A. 2008. Innate immunity to
624 Paracoccidioides brasiliensis infection. Mycopathologia 165:223-36.

625 29. Deepe GS, Jr., Gibbons RS, Smulian AG. 2008. Histoplasma capsulatum
626 manifests preferential invasion of phagocytic subpopulations in murine lungs.
627 J Leukoc Biol 84:669-78.
628 30. Van Prooyen N, Henderson CA, Hocking Murray D, Sil A. 2016. CD103+
629 Conventional Dendritic Cells Are Critical for TLR7/9-Dependent Host Defense
630 against Histoplasma capsulatum, an Endemic Fungal Pathogen of Humans.
631 PLOS Pathogens 12:e1005749.
632 31. Szymczak WA, Deepe GS, Jr. 2010. Antigen-presenting dendritic cells rescue
633 CD4-depleted CCR2-/- mice from lethal Histoplasma capsulatum infection.
634 Infect Immun 78:2125-37.
635 32. Allen HL, Deepe GS, Jr. 2005. Apoptosis modulates protective immunity to the
636 pathogenic fungus Histoplasma capsulatum. J Clin Invest 115:2875-85.
637 33. Kugler S, Schurtz Sebghati T, Groppe Eissenberg L, Goldman WE. 2000.
638 Phenotypic variation and intracellular parasitism by Histoplasma capsulatum.
639 Proc Natl Acad Sci U S A 97:8794-8.
640 34. Rice P, Longden I, Bleasby A. 2000. EMBOSS: the European Molecular
641 Biology Open Software Suite. Trends Genet 16:276-7.
642 35. Concordet JP, Haeussler M. 2018. CRISPOR: intuitive guide selection for
643 CRISPR/Cas9 genome editing experiments and screens. Nucleic Acids Res
644 46:W242-W245.
645 36. Retallack DM, Heinecke EL, Gibbons R, Deepe GS, Jr., Woods JP. 1999. The
646 URA5 gene is necessary for histoplasma capsulatum growth during infection
647 of mouse and human cells. Infect Immun 67:624-9.
648 37. den Dulk-Ras A, Hooykaas PJ. 1995. Electroporation of Agrobacterium
649 tumefaciens. Methods Mol Biol 55:63-72.

650

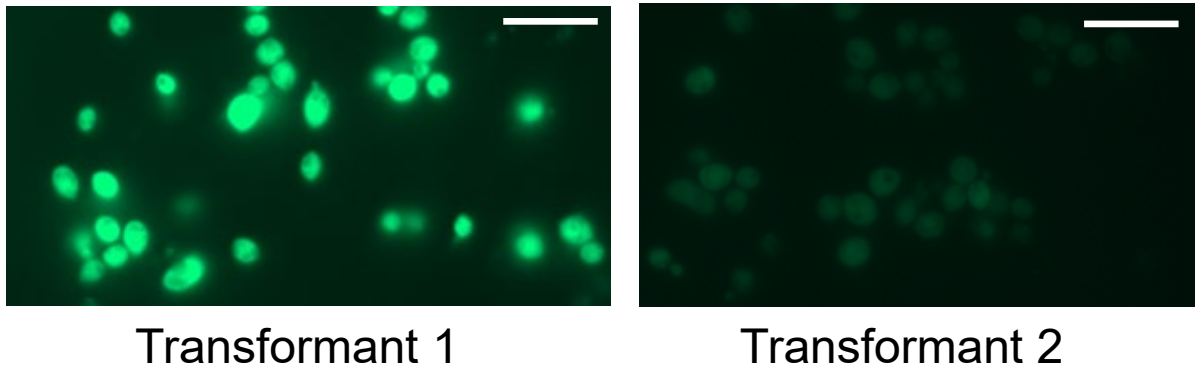

Figure 1: GFP-expressing E. africanus derived through ATMT. E. africanus GFP-expressing transformants were derived by transformation with A. tumefaciens harbouring pAG22. Individual transformant colonies were evaluated by fluorescence microscopy, showing variable expression levels of GFP between transformants under constant imaging conditions. Bar=10μm

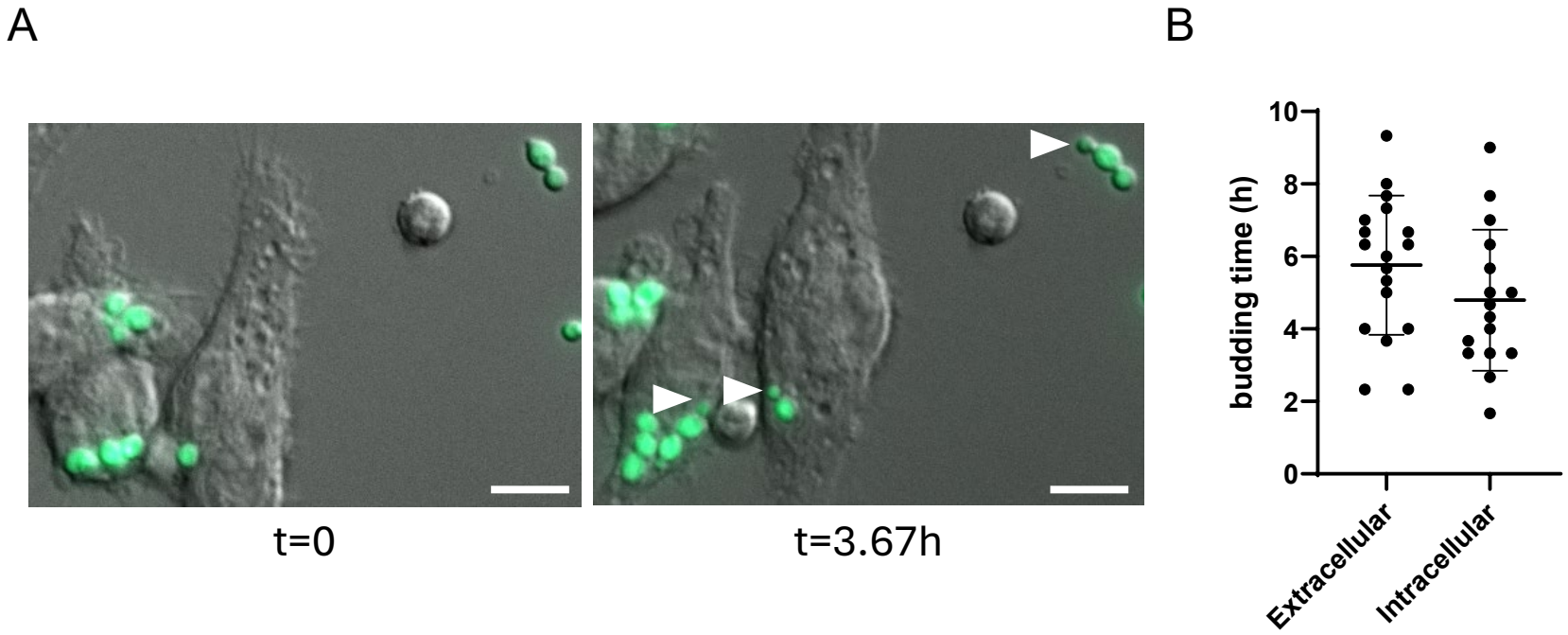

Figure 2: An *E. africanus* GFP fluorescent reporter strain facilitates the study of intracellular yeast growth
GFP fluorescent reporter yeast was added to J774.1 macrophage cells in chambered imaging slides. Time-lapse imaging was started 1 hour after yeast addition (t=0), at which point several yeast cells had been internalised (a representative example is shown in A, left). The emergence of new buds (A, right, indicated by arrows) was recorded. Observed budding time was summarised for several fields of view that contained a mix of both extracellular and intracellular yeasts, $P>0.05$ (mean ± SD). Bar=10μm.

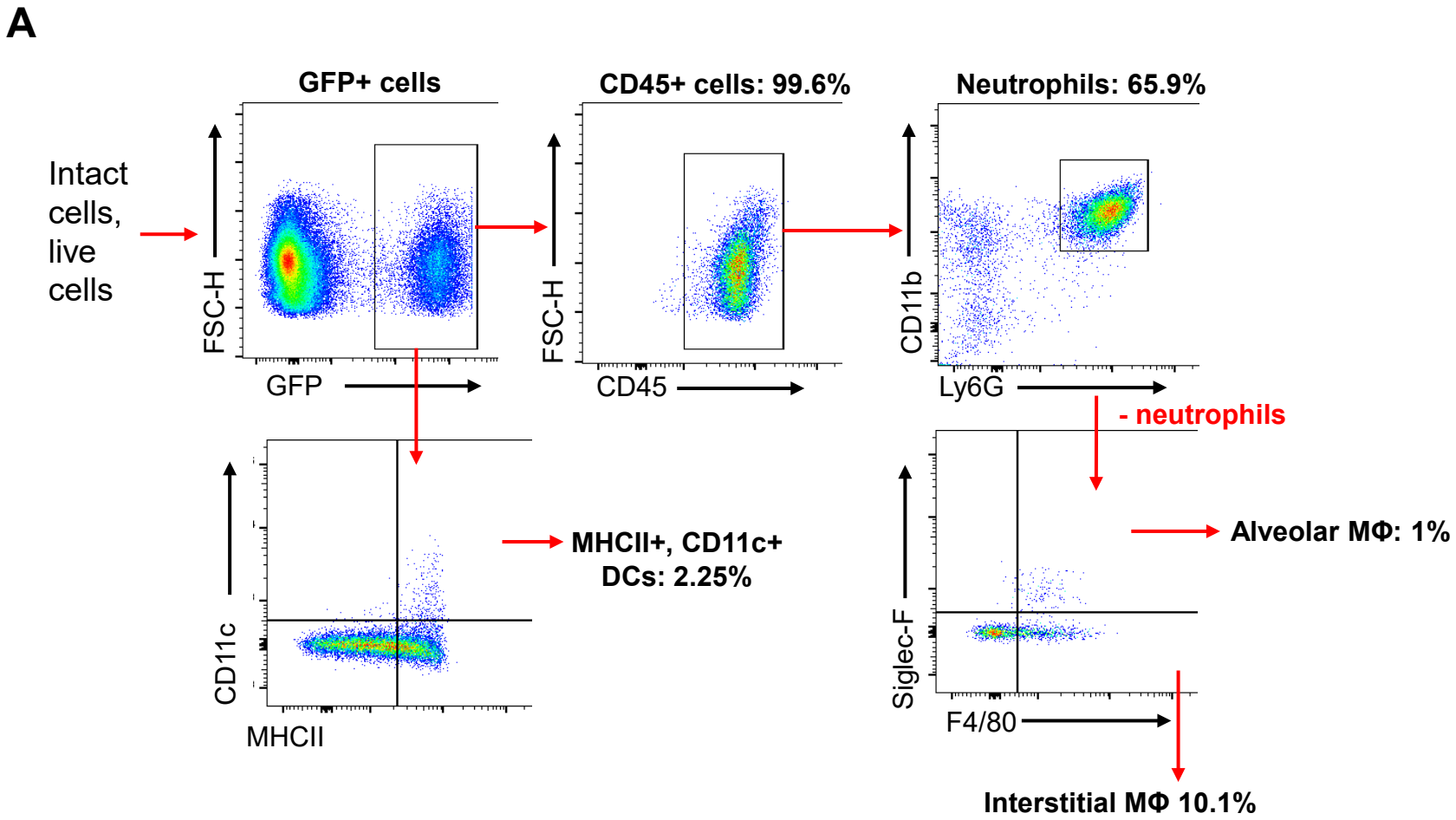
A
Intact cells, live cells
GFP+ cells
FSC-H
GFP
CD45+ cells: 99.6%
FSC-H
CD45
Neutrophils: 65.9%
CD11b
Ly6G
- neutrophils
MHCII+, CD11c+
DCs: 2.25%
CD11c
MHCII
Alveolar MΦ: 1%
Siglec-F
F4/80
Interstitial MΦ 10.1%

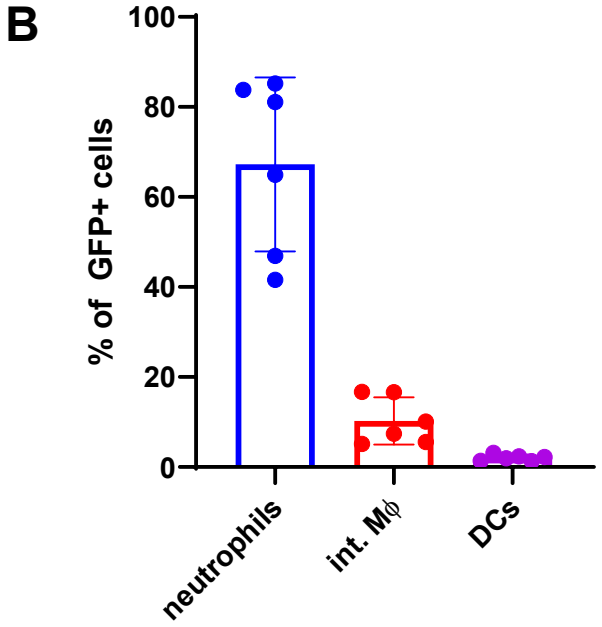
B
% of GFP+ cells
100
80
60
40
20
0
neutrophils
int. Mϕ
DCs

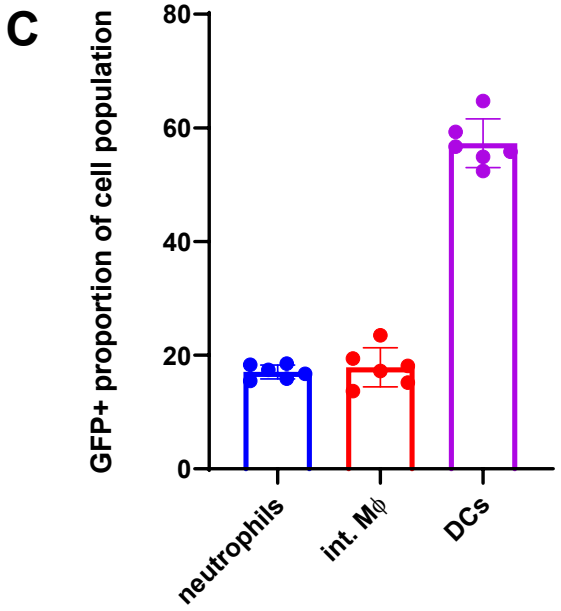
C
GFP+ proportion of cell population
80
60
40
20
0
neutrophils
int. Mϕ
DCs

D

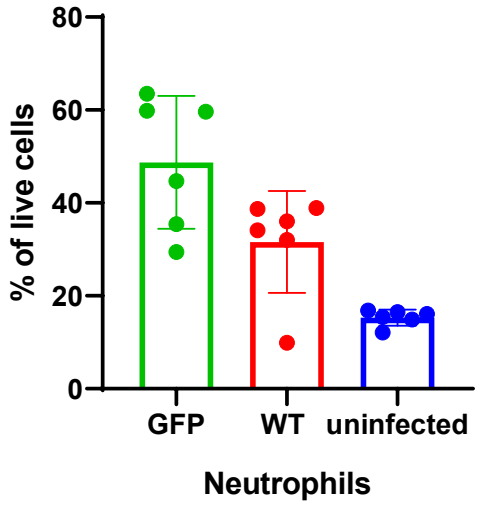
80
60
40
20
0
% of live cells
GFP
WT
uninfected
Neutrophils

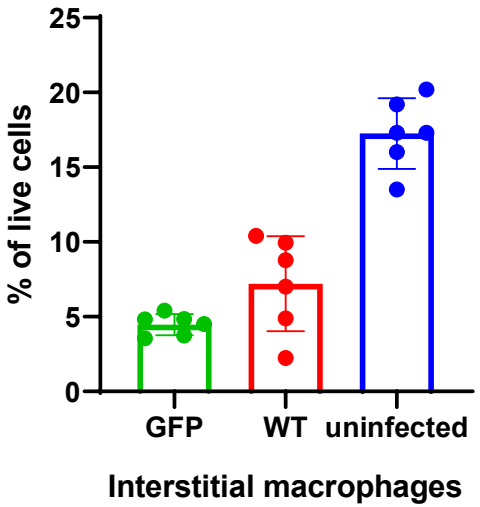
25
20
15
10
5
0
% of live cells
GFP
WT
uninfected
Interstitial macrophages

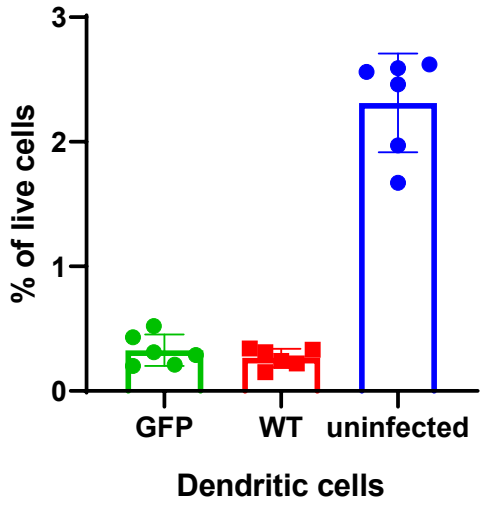
3
2
1
0
% of live cells
GFP
WT
uninfected
Dendritic cells

Figure 3: Identification of myeloid cell types associated with GFP-expressing E. africanus in mouse lung at 7 days post-infection. Scatter plots showing the strategy of gating on GFP first (A), which was used to identify myeloid cell types in the mouse lung that were GFP-positive (associated with the GFP reporter yeast), as summarised in (B). (C) Alternate gating on the various cell types first determined the proportions of each cell type associated with GFP yeast. (D) Myeloid cell distribution in the WT-and and GFP strain-infected mouse lung and in uninfected mouse lung. Differences in cell recruitment between WT- and GFP-strain-infected mice were not significant, $P>0.05$ (mean ± SD). n=6 mice per group, data is representative of two independent experiments.

A

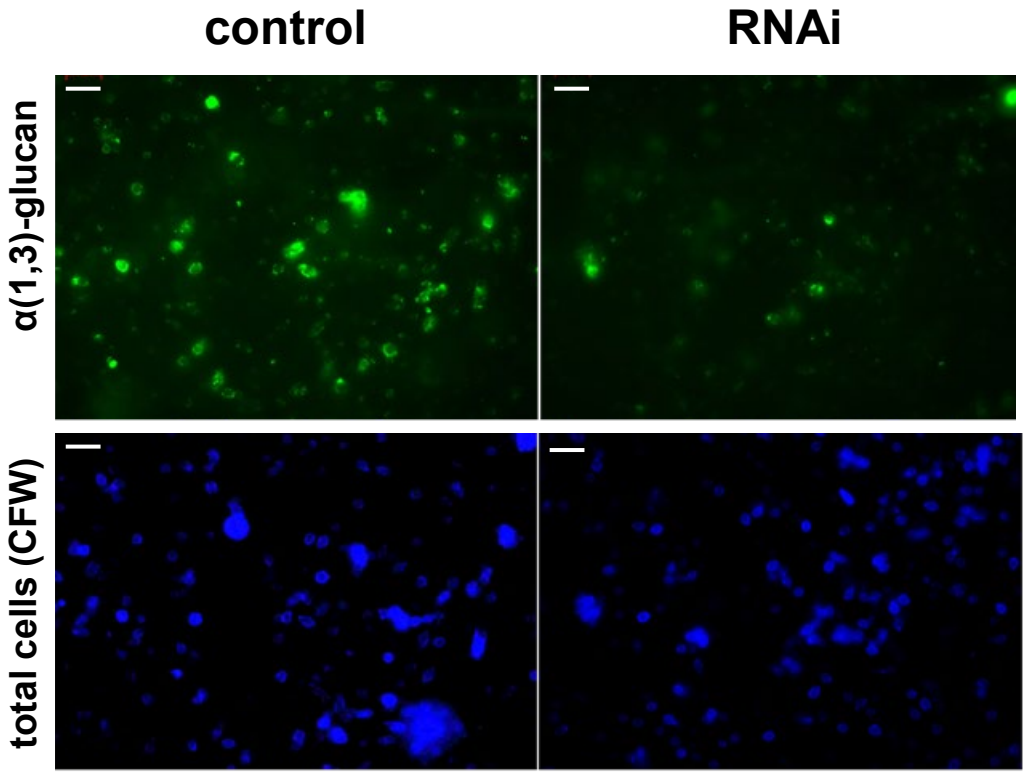
control
RNAi
α(1,3)-glucan
total cells (CFW)

B

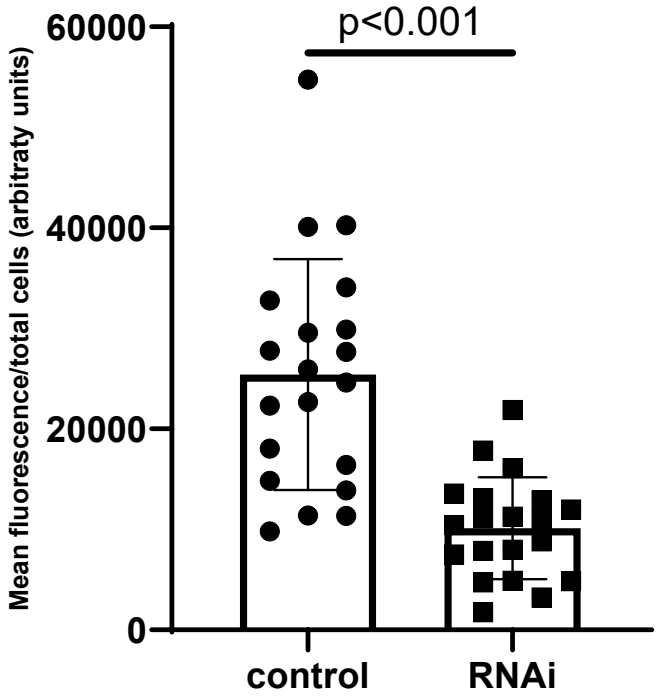
p<0.001
60000
40000
20000
0
Mean fluorescence/total cells (arbitraty units)
control
RNAi

Figure 4: (A) Cell wall staining and fluorescence microscopy of wild-type and AGS1 RNAi strains of E. africanus. E. africanus harbouring the AGS1 RNAi plasmid or the control GFP RNAi plasmid were stained with a monoclonal antibody specific for α(1,3)-glucan and calcofluor white (CFW) and examined by fluorescence microscopy. Imaging settings were kept constant for all samples. Bar=10μm (B) Background-corrected mean fluorescence intensity of microscopy images was measured and normalised by the number of cells per image. Ten images each from two independent experiments were analysed, (mean ± SD) Student's unpaired t-test, $p<0.001$.

A

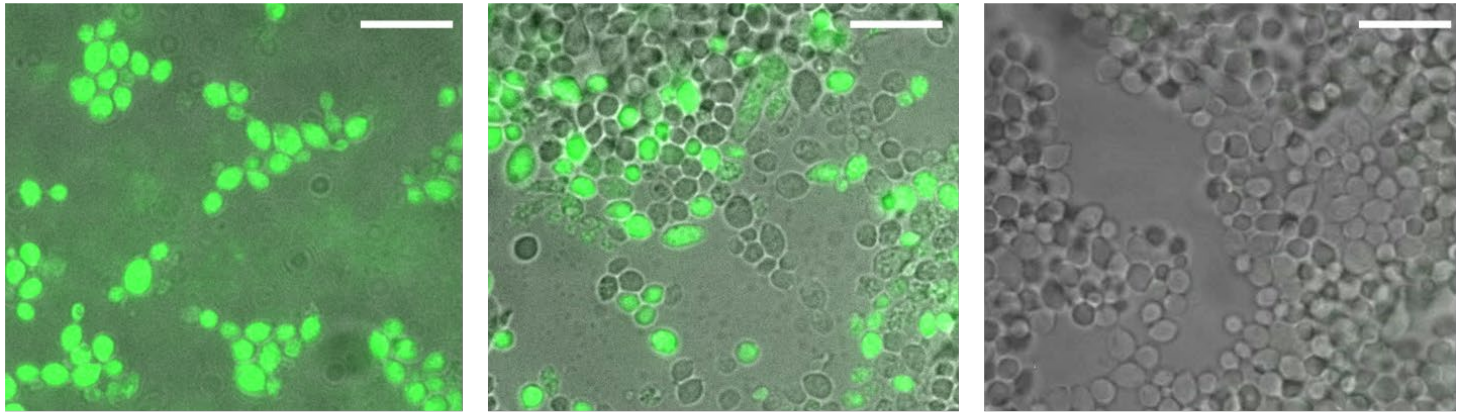

B

Sequencing: GFP-F

expected Cas9 cut site

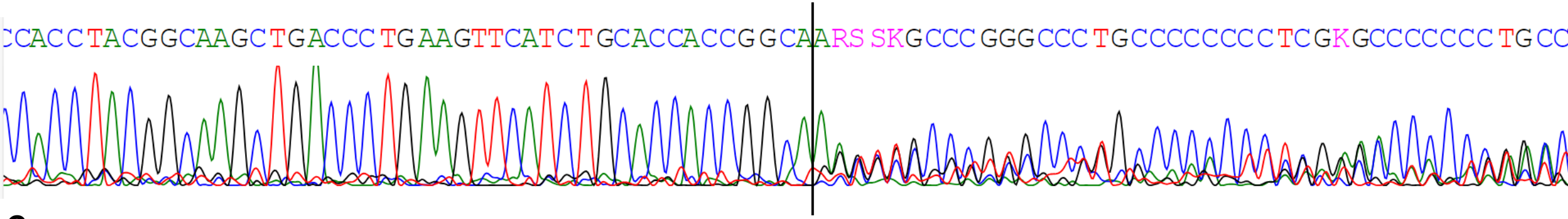

C

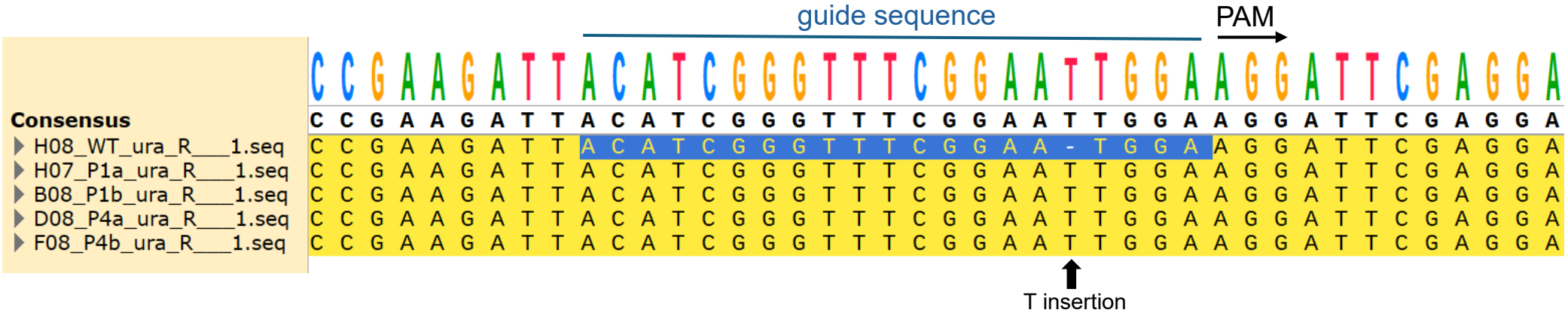

Figure 5: Evaluation of a CRISPR/Cas9 episomal system in E. africanus. (A) Merged fluorescence microscopy and brightfield images showing a decline in the proportion of fluorescent yeast cells with subsequent passages following transformation of GFP-expressing E. africanus with the CRISPR/Cas9 plasmid pSL01-sgGFP. Bar=10µm. (B) Sanger sequencing of a mixed population showed a mixture of signals following the expected Cas9 cut site, indicating the presence of various indels in the population. (C) Sequencing data of individually selected clones, aligned with the WT strain, following CRISPR/Cas9-mediated gene disruption of URA5. A T-insertion was observed in all clones.

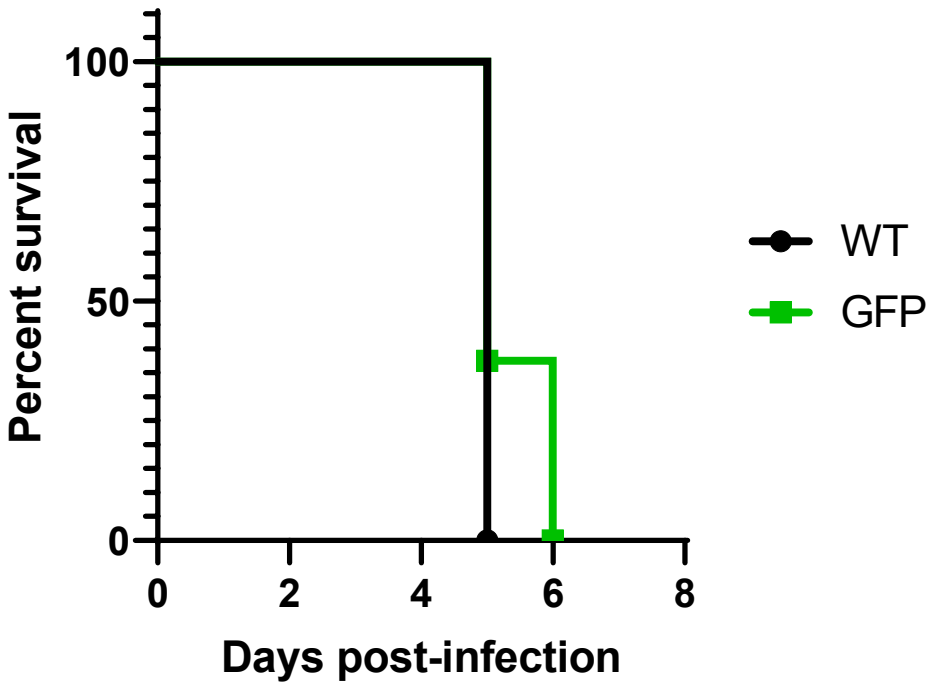
Percent survival
100
50
0
0
2
4
6
8
Days post-infection
WT
GFP

Figure S1: Survival of mice infected with wild-type *E. africanus* and the GFP reporter strain

Mice (n=8 per group) were infected intranasally with a lethal dose of passage-matched wild-type or GFP reporter *E. africanus* yeast cells (2×10^7). Mice were weighed daily and euthanised at the humane endpoint (20% weight loss). The two survival curves are not significantly different, as determined by the log-rank test.

A

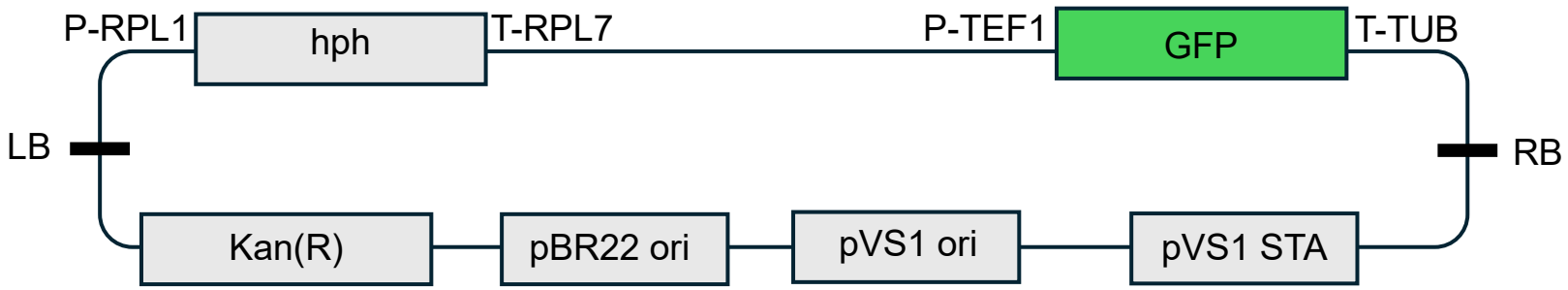
P-RPL1
hph
T-RPL7
P-TEF1
GFP
T-TUB
LB
RB
Kan(R)
pBR22 ori
pVS1 ori
pVS1 STA

B

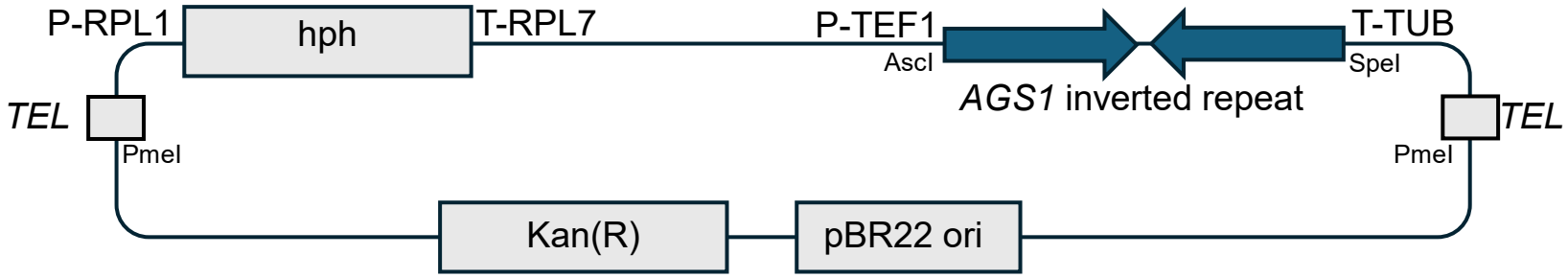
P-RPL1
hph
T-RPL7
P-TEF1
AscI
T-TUB
SpeI
AGS1 inverted repeat
TEL
PmeI
TEL
PmeI
Kan(R)
pBR22 ori

C

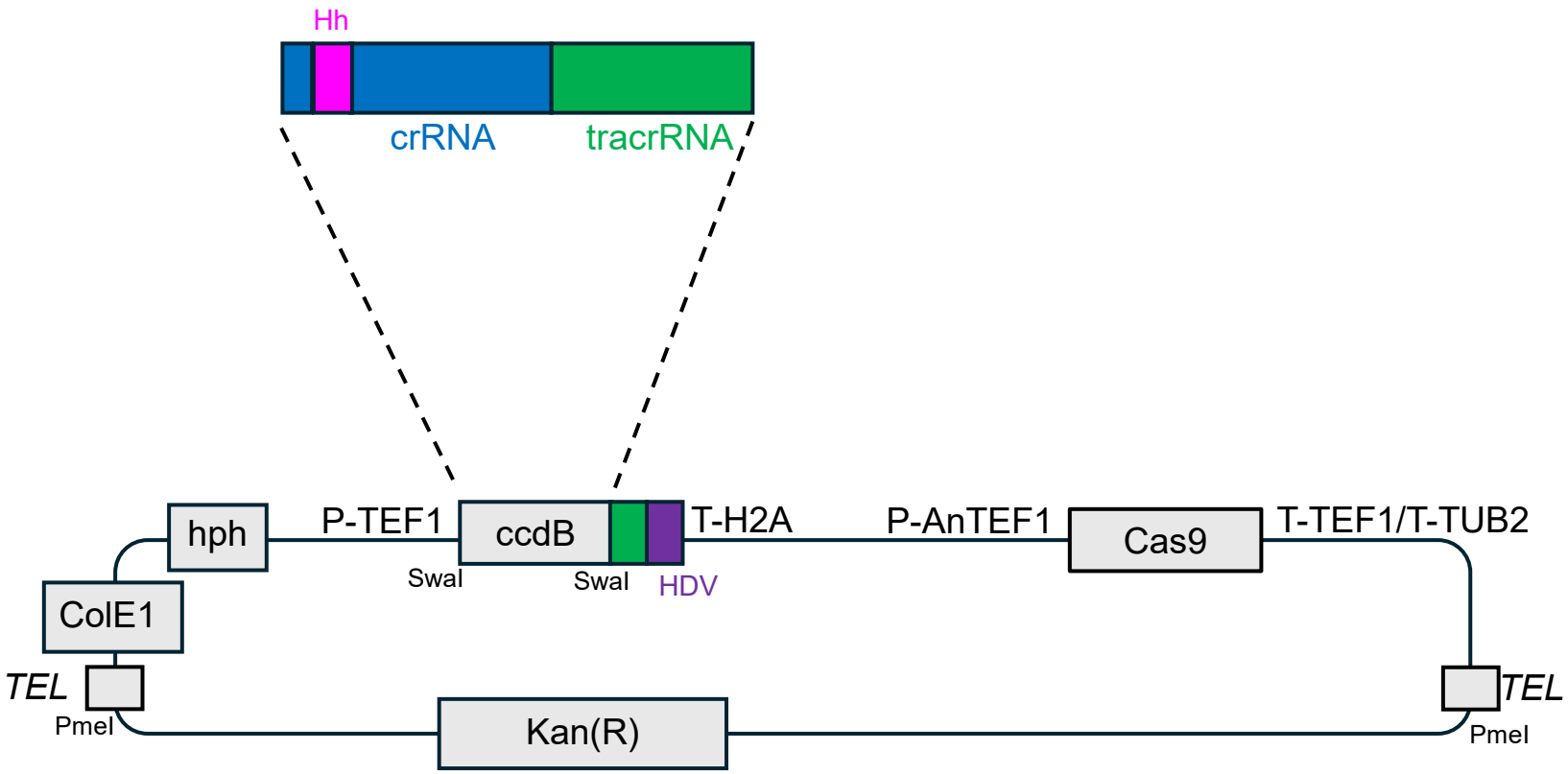
Hh
crRNA
tracrRNA
hph
P-TEF1
ccdB
T-H2A
P-AnTEF1
Cas9
T-TEF1/T-TUB2
SwaI
SwaI
HDV
ColE1
TEL
PmeI
Kan(R)
TEL
PmeI

Figure S2: Schematics of plasmids used in this study with selected features

A: *Agrobacterium* shuttle vector pAG22 contains origins of replication for *E. coli* and *A. tumefaciens,* kanamycin resistance marker, a hygromycin resistance marker under the control of *RPL1* promoter and *RPL7* terminators, and GFP under the control of *TEF1* promoter and *TUB* terminator. LB/RB designate the left- and right borders of the T-DNA. All promoter and terminator sequences are derived from *Histoplasma capsulatum* G217B sequences.

B: Telomeric plasmid with a hygromycin resistance marker used for RNAi. A linearised plasmid with telomere ends (TEL) was generated by PmeI digestion before transforming *E. africanus*. The *AGS1* inverted repeat sequence was derived from the *H. capsulatum* sequence as described in (18).

C: Episomal CRISPR/Cas9 plasmid pSL01, as described in (6), was used to induce frameshift mutations in *E. africanus*. The plasmid was digested with SwaI, and the ccdB marker was replaced by an oligonucleotide containing the *URA5* crRNA sequence with upstream inverted repeat, Hh ribozyme sequence, and part of the tracrRNA sequence, resulting in the expression of a chimeric guide RNA molecule (gRNA), processed by Hh and HDV ribozyme cleavage. The gRNA expression is under the control of the *TEF1* promoter *H2A* terminator derived from *H. capsulatum.* Cas9 expression is driven by the *Aspergillus nidulans TEF1* promoter. The plasmid is linearised by PmeI digestion before transformation of *E. africanus* by electroporation.